Exponential Onset of Scalable Entanglement via Twist-and-Turn Dynamics in XY Models

Tommaso Roscilde,[1] Meenu Kumari,[2,3,4] Alexandre Cooper,[4,5] and Fabio Mezzacapo[1]
[1]*Univ Lyon, Ens de Lyon, CNRS, Laboratoire de Physique, F-69342 Lyon, France*
[2]*Digital Technologies, National Research Council Canada, Ottawa, Canada*
[3]*Perimeter Institute for Theoretical Physics, Waterloo, Ontario, N2L 2Y5, Canada*
[4]*Institute for Quantum Computing, University of Waterloo, Waterloo, Ontario N2L 3G1, Canada*
[5]*Department of Physics and Astronomy, University of Waterloo, Waterloo, Ontario N2L 3G1, Canada*

(Received 25 July 2025; revised 22 July 2026; accepted 13 October 2026; published 19 November 2026)

The efficient preparation of scalable multipartite entanglement is a central goal in the development of next-generation quantum devices. In this work, we show that the so-called "twist-and-turn" (TaT) dynamics for interacting spin ensembles, generated by Hamiltonians with U(1)-symmetric interactions and with a transverse field, can offer an important resource to reach this goal. For models with sufficiently high connectivity, TaT dynamics exhibits two key features: (1) It features both scalable squeezing at short times, as well as quantum Fisher information with Heisenberg scaling at later times, and (2) scalable multipartite entanglement (up to Heisenberg scaling) is reached in a time growing only logarithmically with system size, associated with an exponential buildup of quantum correlations. These results can be shown exactly in the XY model with a Rabi field and infinite-range interactions, and numerically in the case of spatially decaying XY interactions, such as dipolar interactions in two dimensions, provided that unstable spin-wave modes do not develop for large system sizes and/or strong fields. For dipolar interactions, the entanglement dynamics at intermediate times is completely at odds with thermalization, and it appears to saturate the maximum speed of entanglement buildup allowed by Lieb-Robinson bounds generalized to power-law interacting systems.

DOI: 10.1103/74gr-cq5n

Subject Areas: Condensed Matter Physics, Quantum Physics

I. INTRODUCTION

The dynamics of quantum information is a central subject of quantum many-body physics. It dictates fundamental aspects, such as whether and how quantum systems relax to thermal equilibrium [1–3]; whether Hamiltonian evolution can lead to scrambling—i.e., to the impossibility of recovering the initial state if a local perturbation acts on the system before the evolution is run backwards [4–6]; and, most importantly for this work, the ultimate speed at which quantum devices, such as quantum computers and quantum simulators, can prepare and exploit entangled states [7]. A common paradigm in systems with local interactions—e.g., spin chains with short-range couplings—is that of a light-cone propagation of quantum information, or, equivalently, of a ballistic spreading of quantum correlations, regulated by so-called Lieb-Robinson bounds [7]. Within this picture, nearly free quasiparticles act as carriers of quantum information, propagating it at the maximum group velocity of their dispersion relation [8–11]. In contrast, systems in D dimensions with interactions decaying as a power law of the distance r, i.e., as $1/r^{\alpha}$, including the limit of long-range couplings ($\alpha < D$), can exhibit correlations that spread much faster than in systems with finite-range interactions. In particular, for $\alpha < 2D$, the spreading can be exponentially fast, i.e., over distances growing as $\exp(t)$ with time t. This behavior was first predicted as a generalization of Lieb-Robinson bounds to systems with power-law interactions [12,13], and it has been confirmed through the explicit design of protocols generating GHZ-like states using time-dependent power-law interactions [14]. These observations naturally raise the question of whether such an extraordinary fast propagation of quantum correlations can be obtained as well for time-independent Hamiltonians, of relevance to the ongoing effort of quantum simulation of nonequilibrium quantum dynamics [1,3,15].

In this work, we show that a broad class of time-independent Hamiltonians for spin lattices can exhibit an exponential onset of entanglement. Multipartite entanglement emerges from dynamics fundamentally driven by zero-momentum nonlinear excitations (as opposed to finite-momentum quasiparticles). The dynamics under

Published by the American Physical Society under the terms of the Creative Commons Attribution 4.0 International license. Further distribution of this work must maintain attribution to the author(s) and the published article's title, journal citation, and DOI.

consideration is the so-called twist-and-turn (TaT) dynamics [16–20], which has so far been studied only for infinite-range interactions, and which we here generalize to spatially decaying interactions. In the following we shall denote as TaT Hamiltonian (H_{TaT}) a Hamiltonian comprising XY interactions among spins that decay as a power law of the distance, together with an applied Rabi field:

$$H_{\mathrm{TaT}} = -\frac{\mathcal{J}}{\mathcal{N}_\alpha}\sum_{i\neq j}\frac{1}{r_{ij}^\alpha}(S_i^x S_j^x + S_i^y S_j^y) + \Omega\sum_i S_i^x, \quad (1)$$

where S_i^μ ($\mu = x, y, z$) are spin-1/2 operators attached to the sites i of a lattice, which we take to be a $L \times L$ square lattice ($D = 2, N = L^2$) with periodic boundary conditions. We choose the coupling to be ferromagnetic ($\mathcal{J} > 0$), and define the Kac factor as $\mathcal{N}_\alpha = 1 + \sum_{\boldsymbol{r}\neq 0} r^{-\alpha}$ for $\alpha \leq D$ (where $\boldsymbol{r}$ runs over the discrete distances among lattice points), and $\mathcal{N}_\alpha = 1$ otherwise. $\Omega > 0$ is a transverse field chosen to point *opposite* to the orientation of an initial coherent spin state $|\psi(0)\rangle = \otimes |\rightarrow_x\rangle_i$. The Hamiltonian H_{TaT} with infinite-range interactions (i.e., $\alpha = 0$) is known to drive exponentially fast dynamics of entanglement [16,19,20], and it has been implemented experimentally in spinor Bose-Einstein condensates [17,21] as well as in cold gases coupled via a cavity [5]. Yet the scaling behavior of the entanglement properties of the evolved state has only received limited attention theoretically, and it has not been experimentally observed.

Making use of analytical and numerically exact results, as well as of different cross-checked approximations on large lattices, we show that H_{TaT} exhibits an exponentially fast onset of scalable entanglement (namely, entanglement involving a larger number of spins the larger the size) even for power-law interactions, i.e., $\alpha > 0$. In particular, we focus our attention on the case of dipolar interactions ($\alpha = 3$) on square lattices, of immediate relevance to experiments using, e.g., arrays of Rydberg atoms [22], magnetic atoms [23], or dipolar molecules [24]. Several of our results apply as well to interactions decaying more slowly ($\alpha < 3$), and relevant, e.g., to trapped ions [25]. Remarkably, the entanglement generated in the evolution is potentially relevant for metrological applications, both at short times (in the form of squeezing) as well as at longer ones [26]. The longer-term entanglement reaches Heisenberg scaling exponentially in time, i.e., at the quantum speed limit authorized by Lieb-Robinson bounds, over a finite range of sizes, which diverges when the transverse Rabi field vanishes. This scaling, corresponding to long-range entanglement, is completely at odds with the thermodynamics of the system, which is trivialized by the applied field. Hence the entangling dynamics cannot at all be understood as a thermalization process.

Our results show that exponential acceleration of the onset of multipartite entanglement can be achieved across a wide spectrum of quantum devices featuring power-law interactions among their constituents spins—including the above cited platforms (Rydberg atoms, magnetic atoms, dipolar molecules, trapped ions) and beyond. This perspective is particularly appealing, as some of these platforms are achieving a remarkable level of scalability, reaching up to hundreds [27] or even thousands of spins [28] with individual addressing. Yet their limited coherence times may not allow entanglement to spread throughout the system by using conventional dynamics—based, e.g., on short-range interactions, or gates involving only neighboring qubits, which can entangle spins over distances growing only as a power law of time [7]. Nonetheless, this picture may radically change when adopting TaT dynamics, as proposed in this work.

The structure of the paper is as follows. We first discuss the squeezing dynamics and scaling properties of the TaT model with all-to-all interactions (Sec. II). We then report the observation of scalable spin squeezing in the case of dipolar interactions (Sec. III) and describe the emergence of unstable modes in the spin-wave (SW) spectrum at finite wave vector (Sec. IV). We finally explore the onset of multipartite entanglement with Heisenberg scaling at later times (Sec. V), before offering a summary of our findings (Sec. VI).

II. TWIST-AND-TURN DYNAMICS LEADING TO SCALABLE SQUEEZING

For systems with all-to-all interactions ($\alpha = 0$), H_{TaT} is well known to exhibit squeezing at short times, as detected by the squeezing parameter [29],

$$\xi_R^2 = \frac{N\min_\perp \mathrm{Var}(J^\perp)}{\langle J^x\rangle^2}, \quad (2)$$

where $\boldsymbol{J} = \sum_i \boldsymbol{S}_i$ is the collective spin operator, and the numerator is minimized over the collective spin components perpendicular to the net magnetization appearing along the x axis. A state is spin squeezed whenever $\xi_R^2 < 1$. In most of the figures we will express squeezing in decibels (dB); namely, we shall plot $10\log_{10}\xi_R^2$. Squeezing is a fundamental entanglement witness, offering a lower bound to the entanglement depth in the system, i.e., the number k of spins which are entangled together in an irreducible manner: $k \geq \xi_R^{-2}$. And it represents as well the factor by which the quadratic uncertainty in Ramsey interferometry can be reduced thanks to entanglement. In particular, achieving scalable entanglement in the form of squeezing—i.e., a squeezing parameter ξ_R^2 decreasing with system size—can allow Ramsey interferometry to fundamentally beat the scaling of uncertainty imposed by the standard quantum limit, valid for uncorrelated spins [29].

The uncertainty region on the Bloch sphere of the initial, coherent spin state is rotationally symmetric around the x axis; however, it gets deformed by the dynamics generated

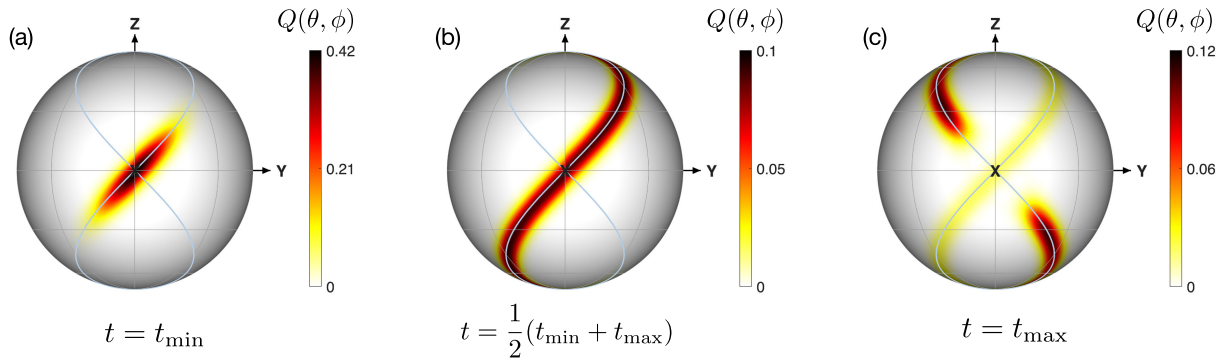


FIG. 1. Twist-and-turn dynamics (TaT). We represent the Husimi function $Q(\theta,\phi) = |\langle\theta,\phi|\psi\rangle|^2$ for three different times of the twist-and-turn dynamics with all-to-all interactions and $\Omega = 0.5\mathcal{J}$. Here $|\theta,\phi\rangle$ is a coherent spin state oriented along the direction defined by the (θ,ϕ) angles on the Bloch sphere. We represent three times of the TaT evolution: (a) the time of optimal squeezing, $t_{\min}$, (c) the time of maximum quantum Fisher information $\mathrm{QFI}(J^y)$, $t_{\max}$, and (b) the half time between the two previous times. The eight-shaped line on the Bloch sphere is a classical separatrix, corresponding to the trajectory which contains the hyperbolic fixed point $(X,Y,Z) = (1,0,0)$, of the classical TaT Hamiltonian. All calculations were made for $N = 200$ spins.

by H_{TaT}, with the spin-spin interaction term leading to "twisting" of the collective spin (i.e., to a rotation around the z axis in the northern hemisphere, or around the $-z$ axis in the southern hemisphere), and the transverse field term leading to "turning" of the spin around the x axis [17]; see Fig. 1 for an illustration of the twist-and-turn dynamics using Husimi functions. As discussed in Ref. [19], in the classical limit of a collective spin of infinite length, and for $0 < \Omega < \mathcal{J}$, the positive x direction represents a hyperbolic fixed point. Its directions of stability and instability correspond to exponential squeezing [see Figs. 1(a) and 2(a)] and antisqueezing, respectively, with a rate $\lambda = \sqrt{\Omega(\mathcal{J}-\Omega)}$.

At the quantum mechanical level, exponential squeezing and antisqueezing at short times with the same exponent λ can be obtained by mapping the collective spin (of fixed length $J = N/2$) onto a bosonic mode—see Appendix A for a detailed derivation—namely, $\min_{\perp}\mathrm{Var}(J^{\perp}) \approx (N/4)e^{-2\lambda t}$. The fastest squeezing dynamics is therefore achieved for the optimal field $\Omega_o/\mathcal{J} = 1/2$. Nonetheless, squeezing dynamics is found to stop at times $t_{\min} \sim (1/\lambda)\log\sqrt{N}$ [Figs. 2(a) and 2(c)] [19], and to lead therefore to an optimal squeezing scaling as $(\xi_R^2)_{\mathrm{opt}} \sim 1/\sqrt{N}$. This scaling behavior is a fundamental feature of TaT dynamics, previously reported for weak fields [30]. Here, using exact diagonalization, it is found to be universal across the entire field interval $0 < \Omega < \mathcal{J}$, as shown in Fig. 2(b). Compared with one-axis-twisting (OAT) dynamics (corresponding to the case $\alpha = 0$, $\Omega = 0$), TaT squeezing dynamics leads to a weaker scaling of optimal squeezing: $\xi_R^2 \sim N^{-1/2}$ for TaT vs $\xi_R^2 \sim N^{-2/3}$ for OAT [31]. However, TaT dynamics has the advantage that this optimal squeezing is reached in a time that grows only logarithmically with system size, due to an exponential buildup of spin squeezing at short times.

III. DIPOLAR TWIST-AND-TURN SQUEEZING

We now consider power-law decaying interactions, focusing on the case of dipolar interactions ($\alpha = 3$) in two dimensions. Such interactions allow the dynamics to leak out of the Dicke sector of maximal spin length $\langle \boldsymbol{J}^2\rangle = N/2(N/2+1)$, and, at least in principle, to relax toward states that reproduce locally the behavior of a thermal state at the energy of the initial state. Thermalization under H_{TaT} would require the magnetization

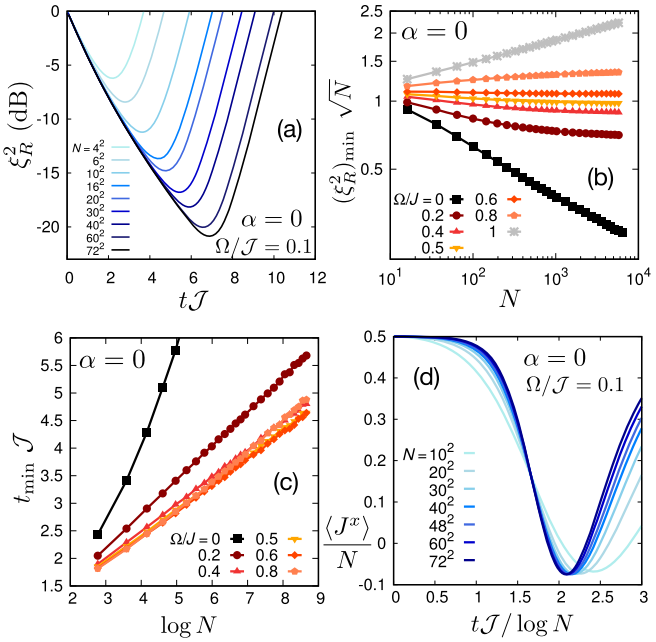


FIG. 2. Twist-and-turn squeezing dynamics with all-to-all interactions. (a) Spin squeezing dynamics for $\Omega = 0.1\mathcal{J}$, (b) optimal squeezing and (c) time to optimal squeezing for the TaT dynamics with all-to-all interactions, (d) magnetization dynamics for $\Omega = 0.1\mathcal{J}$. All data stem from exact calculations.

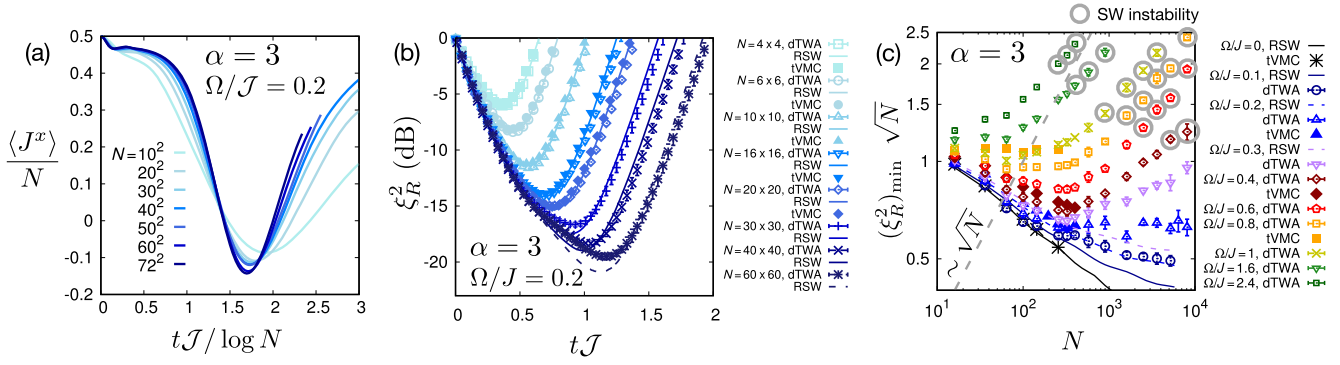


FIG. 3. Twist-and-turn squeezing dynamics with dipolar interactions. (a) Dynamics of the magnetization of the 2D dipolar model with $\Omega/\mathcal{J} = 0.2$ (dTWA data). (b) Squeezing dynamics for the dipolar 2D system with $\Omega/\mathcal{J} = 0.2$, from dTWA, RSW, and tVMC. (c) Scaling of the optimal squeezing for different values of the field. The dashed gray line indicates the $\sqrt{N}$ behavior, corresponding to the absence of scalable squeezing. Squeezing parameters showing a slower power-law scaling than that of the gray line imply the presence of scalable squeezing. The gray circles highlight field and size values for which imaginary spin-wave (SW) frequencies have appeared.

to reverse its orientation (to align with the field), and the excess Rabi energy to be dumped into the interaction term, thereby suppressing correlations (more on this aspect in Sec. V B).

Yet, this is not at all what is observed. To reconstruct the dynamics of the dipolar system, we employ a joint numerical strategy based on the systematic comparison between the discrete truncated Wigner approximation (dTWA) [32] and the time-dependent variational Monte Carlo (tVMC) method using the pair-product ansatz [33,34], augmented with a wave function term that depends on the total magnetization [35]. Both these approaches have been recently shown to provide quantitative predictions for the quench dynamics of dipolar XY models at low energies [36,37]. We interpret the agreement between them as a strong indication of the quantitive nature of our results.

For sufficiently small fields, the magnetization dynamics of the dipolar system remains close to that of an all-to-all coupled system [Fig. 2(d)], but with an effective coupling constant $\mathcal{J}_{\text{eff}} = \mathcal{J}\sum_{r\neq 0} r^{-\alpha}$—i.e., with an interaction term of the kind $(\mathcal{J}_{\text{eff}}/N)[(J^x)^2 + (J^y)^2]$. And the magnetization partially reverses direction over a time scaling as $\log N$; see Fig. 3(a). This dynamics leaves ample time for squeezing correlations to build up within a timescale growing also logarithmically with size, and for optimal squeezing to reach the same scaling as in the $\alpha = 0$ case. In Figs. 3(b) and 3(c), we clearly observe this behavior for $\Omega/\mathcal{J} = 0.2$ using both the above-mentioned numerical approaches, and up to very large system sizes ($L = 90$ using dTWA).

This behavior is also quantitatively captured by a rotor-spin-wave (RSW) separation scheme [38], which describes the dynamics in the Dicke sector exactly as that of the $\alpha = 0$ model with $\mathcal{J}_{\text{eff}}$ coupling—and treats the leakage of the dynamics from the Dicke sector within a spin-wave approximation; see Appendix B for an extended discussion. RSW theory deviates from dTWA for very large sizes ($N \gtrsim 30^2$), as the two theories predict a change in the exponential decay of squeezing below -15 dB, but with a different exponent [see Fig. 3(b)]. This discrepancy might be understood in that the assumption of decoupling between rotor and spin-wave degrees of freedom, at the basis of RSW, is too rough, and a weak coupling still exists, affecting the squeezing dynamics, but not altering its overall scaling properties at sufficiently small fields Ω.

A comprehensive picture of the scaling of the optimal squeezing for various fields is provided in Fig. 3(c). There we observe that, for sufficiently small fields ($\Omega/\mathcal{J} \lesssim 0.2$), optimal squeezing appears to maintain the same asymptotic scaling as in the $\alpha = 0$ case, namely, $(\xi_R^2)_{\min} \sim N^{-\nu}$ with $\nu = 1/2$. For larger fields, optimal squeezing remains scalable, but its asymptotic scaling appears to become field dependent, with a ν exponent decreasing gradually with Ω. Determining the field at which scalability is entirely lost is rather difficult. Nonetheless, it is clear that scalable spin squeezing is observed in the dipolar dynamics, in spite of the emergence of unstable spin-wave modes, as we shall discuss in the next section.

IV. SPIN-WAVE INSTABILITIES

A peculiar feature of RSW theory applied to TaT dynamics is that it is built around an *unstable* fixed point of the classical dynamics [19]. In systems with spatially decaying interactions, the same instability that affects the dynamics of the zero-momentum degrees of freedom, leading to its exponential acceleration, can also affect that of the finite-momentum (i.e., spin-wave) modes. Indeed, for sufficiently large sizes, the spin-wave frequencies of the dipolar XY model at small wave vector ($|\boldsymbol{k}| \sim 1/L$) can become imaginary $\omega_{\boldsymbol{k}} = i\lambda_{\boldsymbol{k}}$; see Appendix B for a detailed discussion.

Figure 4(a) shows the range of fields and sizes at which unstable SW modes appear for the 2D dipolar case. As discussed in Appendix B, an instability at finite momentum

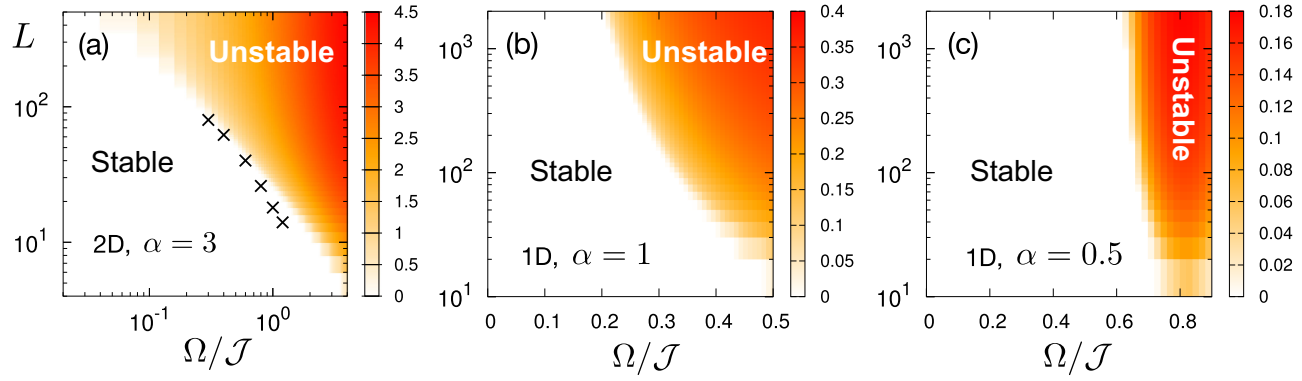


FIG. 4. Stability diagram of spin waves. (a) Dipolar interactions ($\alpha = 3$) in 2D. The false colors indicate the largest imaginary spin-wave frequency at finite wave vector $\lambda_{\max} = \max_{\boldsymbol{k}\neq 0} \mathrm{Im}(\omega_{\boldsymbol{k}})$, as a function of the applied field Ω and the linear system size L. The crosses indicate the estimated crossover in the scaling of $\mathrm{Var}(J^y)_{\max}$; see Fig. 9. (b) Coulomb interactions ($\alpha = 1$) in 1D and (c) long-range interactions ($\alpha = 0.5$) in 1D. Same significance of false colors as in (a). The difference in field ranges and values of $\lambda_{\max}$ between panel (a) and panels (b) and (c) should be mainly attributed to the different Kac normalization (see main text).

occurs for a field value which pushes the frequency of the mode at the lowest wave vector [$\boldsymbol{k} = (2\pi/L, 0)$ on a square lattice] to imaginary values. This condition is met when the field exceeds a critical value,

$$\left(\frac{\Omega}{\mathcal{J}}\right)_c (L) \sim L^{-2z} \quad (L \gg 1), \tag{3}$$

where z is the dynamical exponent dictating the dispersion relation at zero field of the system at long wavelength, $\omega \sim k^z$. For the models of interest to this work, $z = 1$ for $\alpha \geq D + 2$, $z = (\alpha - D)/2$ for $D < \alpha < D + 2$, and $z = 0$ for $\alpha \leq D$ [39].

For the moderate fields on which we focus our discussion, the instability in the modes of the dipolar system occurs for very large system sizes—e.g., above $N \approx 10^2 \times 10^2$ for $\Omega/\mathcal{J} = 0.2$. Interestingly, Fig. 3(c) shows that scalable optimal squeezing persists even for sizes and fields at which the SW spectrum develops unstable modes. This aspect can be related to the fact that the exponential rate of proliferation of low-k spin waves $\lambda_{\boldsymbol{k}}$ remains systematically smaller than the rate λ of increase of the zero-mode fluctuations, hence affecting only mildly the early dynamics of the system. The dTWA data of Fig. 3(c) suggest a clear crossover in the scaling properties for intermediate sizes, which could be interpreted as a signature of the onset of unstable modes. Yet, as we show in Appendix C, at the optimal squeezing time no clear dynamical instability is observed for the system sizes we investigated, since the collective spin remains firmly polarized $\langle J^x \rangle \sim O(N)$. The change in scaling of optimal squeezing is rather due to $\min_\perp \mathrm{Var}(J^\perp)$ changing its exponentially decaying dynamics [as seen in Fig. 3(b) for the largest system sizes]. As we shall see below, unstable modes have instead a clearer impact on the later dynamics of entanglement.

It is important to point out that, for $\alpha < D$, the critical field loses its size dependence in Eq. (3); namely, there is a whole range of field values for which spin waves built around an unstable point are actually stable harmonic modes for all system sizes. Figures 4(b) and 4(c) show the stability diagram for interactions with $\alpha = 1$ (Coulomb) and $\alpha = 0.5$ in 1D, both relevant to trapped ion chains [25]. The Coulomb case is marginal, i.e., it sits at the boundary between short-ranged interactions and long-ranged ones, and it shows a logarithmic dependence of the critical field on the system size. On the other hand, in the case $\alpha = 0.5$ in $D = 1$, corresponding to long-range interactions, the size dependence of the critical field essentially disappears. This implies that there exists an entire class of models with power-law decaying interactions for which the TaT dynamics of the $\alpha = 0$ limit is potentially stable for all system sizes.

V. TWIST-AND-TURN DYNAMICS LEADING TO HEISENBERG SCALING OF ENTANGLEMENT

A. All-to-all interactions

We now focus our attention on the entangling dynamics after squeezing is lost. As seen in Sec. II, the exponential squeezing of the minimum variance stops at a time $\sim \log(\sqrt{N})$. Yet, as shown in Fig. 5(a) for the case $\alpha = 0$, the most fluctuating collective-spin component transverse to the net magnetization keeps growing exponentially as $\max_\perp \mathrm{Var}(J^\perp) \approx (N/4)e^{2\lambda t}$, and up to longer times $t \sim \log N$ [19], reaching therefore *Heisenberg scaling* of entanglement. This dynamics is observed for the entire range of fields $\Omega \in (0, \mathcal{J})$, in agreement with previous studies [5,19] and with the analytical treatment we provide in Appendix A. Figure 5(b) shows the exponential growth of $\mathrm{Var}(J^y)$ up to Heisenberg scaling in a time scaling as $\log N$, and the Heisenberg scaling of the maximum of $\mathrm{Var}(J^y)$ for the field range $\Omega \in (0, \mathcal{J})$ is shown in Fig. 5(b). The maximum of $\mathrm{Var}(J^y)$ reaching Heisenberg scaling corresponds to a collective-spin state (depicted in Fig. 1 via

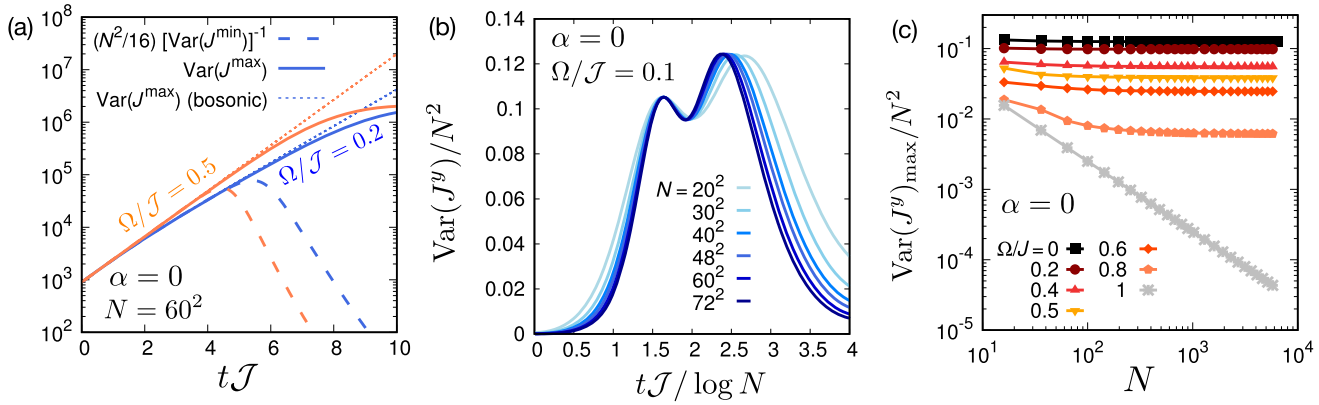


FIG. 5. Twist-and-turn exponential buildup of long-range entanglement. (a) Exponential dynamics of the variances of the squeezed ($J^{(\mathrm{min})}$) and antisqueezed ($J^{(\mathrm{max})}$) collective-spin component for $\alpha = 0$ and two field values. The thin dashed line corresponds to the squeezing dynamics of the bosonic model obtained by linearized Holstein-Primakoff mapping of the collective spin. (b) Dynamics of $\mathrm{Var}(J^y)$ for $\Omega = 0.1\mathcal{J}$. (c) Scaling of the peak of $\mathrm{Var}(J^y)$ for $\alpha = 0$. The value corresponds to the second local maximum for $\Omega > 0$ [see (b)] and to the plateau value for $\Omega = 0$.

the Husimi function) which accumulates on regions of the classical trajectory that are opposite in the J^y spin component; see Fig. 1(c).

$\mathrm{Var}(J^y)$ corresponds to the quantum Fisher information (QFI) for pure states, $\mathrm{QFI}(J^y) = 4\mathrm{Var}(J^y)$, and its scaling as N^2 implies Heisenberg scaling of multipartite entanglement [29]. In fact, the QFI per spin offers a lower bound to the entanglement depth k, $k \geq \mathrm{QFI}(J^y)/N$. Hence a QFI scaling as N^2 certifies that a macroscopic [i.e., $O(N)$] fraction of the N spins in the system are entangled with each other. Moreover, the QFI bounds the minimal quadratic uncertainty that arbitrary measurements on the quantum state of the system can achieve in reconstructing the phase ϕ of a rotation around the y axis, $U(\phi) = e^{-iJ^y\phi}$: $(\delta\phi)^2 \geq 1/\mathrm{QFI}(J^y)$. For the states of interest in this section, this minimal uncertainty can be reached by an explicit metrological protocol, based on the evolution of the parity under rotations [26], as we discuss further in Sec. VI. In fact, Heisenberg scaling of the variance (and related QFI) of all three components of the collective spins is observed, revealing that the collective-spin wave function spreads broadly over the Bloch sphere (see Fig. 1).

B. Dipolar interactions

1. Exponential spreading of correlations

The behavior of the collective spin fluctuations in the 2D dipolar case is instead more complex and intriguing. As shown in Fig. 6, the fluctuations of e.g., the component J^y build up exponentially, and they clearly appear to reach a value consistent with Heisenberg scaling for a sufficiently small field ($\Omega/\mathcal{J} = 0.2$)—in complete analogy with what is seen in the $\alpha = 0$ case. In particular, the maximum value of $\mathrm{Var}(J^y)$ lies above that reached by OAT-like dynamics (i.e., for $\Omega = 0$); and nonetheless it is reached in a time scaling only logarithmically with system size. This conclusion can be easily drawn thanks to the agreement between the timing of the maximum predicted by dTWA and that predicted by RSW theory. The latter theory predicts indeed that $\mathrm{Var}(J^y)$ is the same as that of an all-to-all interacting model (the rotor) [40], with an effective coupling related to the dipolar interactions [see Eq. (B6) in Appendix B]. Hence the logarithmic scaling of the peak time observed in Fig. 5(b) applies to the dipolar model as well; see Fig. 6(d). This observation implies that TaT dynamics shows exponential acceleration toward Heisenberg scaling compared to OAT-like dynamics, obtained for zero field. The latter reaches indeed Heisenberg scaling in a much longer time, $t \sim \sqrt{N}$ [29], as shown in Fig. 6(e).

At variance with the $\alpha = 0$ case, the onset of correlations has a peculiar spatial structure, which is rather remarkable. A microscopic insight into the spatial structure of the correlations for the y spin components, $C^{yy}(d,t) = \langle S_i^y S_{i+d}^y\rangle(t)$, which sum up to $\mathrm{Var}(J^y)$, is obtained via our tVMC, dTWA, and RSW calculations; see Fig. 7. All three methods show that, in the dipolar system, correlations advance exponentially in time [i.e., nearly linearly for distances $d \ll L$ when plotted against $\exp(t)$]. This represents the fastest propagation of correlations allowed by Lieb-Robinson bounds in systems with power-law interactions [7,13,14]. Hence dipolar TaT dynamics in 2D offers a paradigmatic example of a simple time-independent Hamiltonian governing time-optimal (i.e., exponential) propagation of quantum information for power-law interactions with $D < \alpha < 2D$.

2. Relationship to thermalization dynamics

It is important to stress that this exponential buildup of long-range correlations discussed above has no relationship to thermalization dynamics, which is not at all observed in

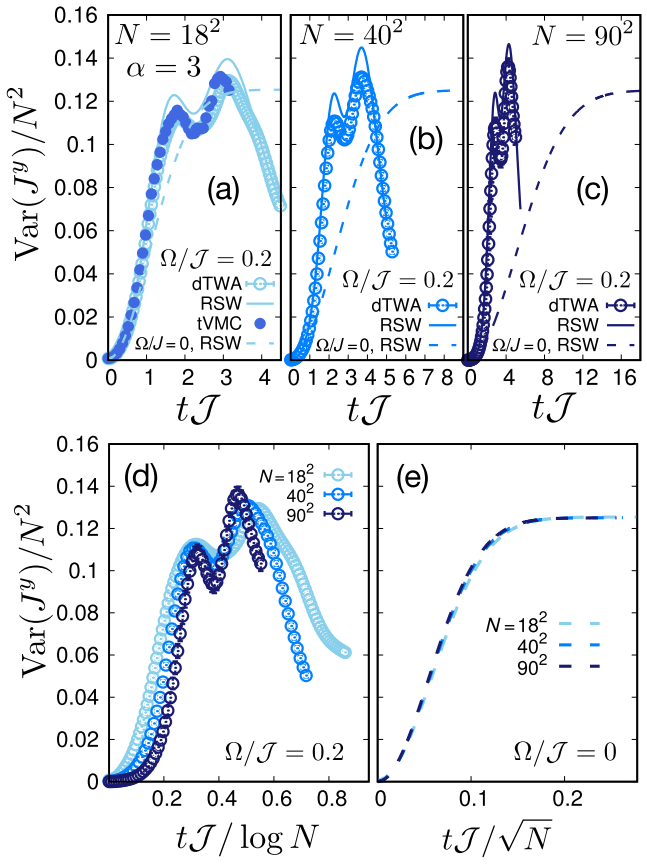


FIG. 6. Exponential onset of entanglement in the 2D dipolar model. (a)–(c) Dynamics of $\mathrm{Var}(J^y)$ for the 2D dipolar model with $\Omega/\mathcal{J} = 0.2$ from RSW, dTWA, and tVMC, for three different system sizes. The OAT case ($\Omega = 0$) is also shown for comparison. (d) The dTWA data for $\Omega/\mathcal{J} = 0.2$ are plotted as a function of $t\mathcal{J}/\log(N)$, exposing the logarithmic scaling of the time at which Heisenberg scaling of entanglement is achieved. (e) On the other hand, the data for $\Omega/\mathcal{J} = 0$ achieve Heisenberg scaling in a time scaling as $\sqrt{N}$, as shown by plotting the corresponding data as a function of $t\mathcal{J}/\sqrt{N}$.

the time range we focused on. The thermal behavior of the TaT Hamiltonian is completely trivial: At the temperature related to the energy of the initial state, the applied field, coupling to the order parameter of the system, very strongly polarizes the system, and correlations are short-ranged for all spin components. Using the quantum Monte Carlo (QMC) method [41], we calculate the thermodynamics expected at a temperature ($T/\mathcal{J} \approx 2.2$) corresponding to the energy of the initial coherent spin state for $\Omega/\mathcal{J} = 0.2$; namely, $\langle H\rangle_T = \langle\psi(0)|H|\psi(0)\rangle$. The magnetization is expected to be $\langle J^x\rangle/N \approx -0.46$, completely at odds with anything to be seen in Fig. 3(a), and correlations are short-ranged, giving $\mathrm{Var}(J^y) \approx 5.2N$. Therefore the dynamical onset of long-range correlations in this system is a genuine nonequilibrium effect.

We highlight this important aspect in Fig. 8(a), showing the evolution of the structure factor for the y spin component:

$$\mathcal{S}^{yy}(\boldsymbol{k}) = \frac{1}{N}\sum_{ij} e^{i\boldsymbol{k}\cdot(\boldsymbol{r}_i-\boldsymbol{r}_j)}\langle S_i^y S_j^y\rangle, \tag{4}$$

which offers a momentum-space view of correlations. In particular, the zero-momentum peak of the structure factor corresponds to the variance of the J^y collective-spin component: $\mathcal{S}^{yy}(0) = \mathrm{Var}(J^y)/N$ (for $\langle J^y\rangle = 0$, as it is the case here). Figure 8(a) shows that the growth of the structure factor peak along the dipolar TaT dynamics largely overshoots the value expected thermally, as correlations spread all over the system size. On the other hand, thermal correlations, albeit significant for the field value considered here, are short-ranged, i.e., they are exponentially decaying. Figure 8(b) shows the exponential decay of the thermal correlations $C^{yy}(\boldsymbol{r}) = \langle S_i^y S_{i+\boldsymbol{r}}^y\rangle \sim \exp(-r/\xi)$, featuring a characteristic correlation length $\xi \approx 9.5$—this picture should be contrasted with the long-range correlations appearing dynamically, as seen in Fig. 7.

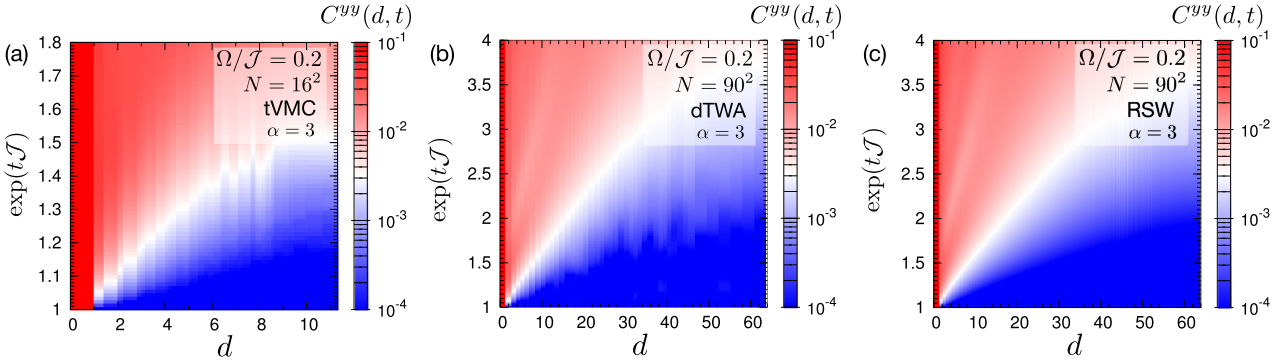


FIG. 7. Exponential spreading of correlations. Dynamics of transverse correlations $C^{yy}(d,t) = \langle S_i^y S_{i+d}^y\rangle(t)$ for the 2D dipolar model with $\Omega/\mathcal{J} = 0.2$ for $N = 16^2$ from tVMC (a) and for $N = 90^2$ from dTWA (b) and RSW (c).

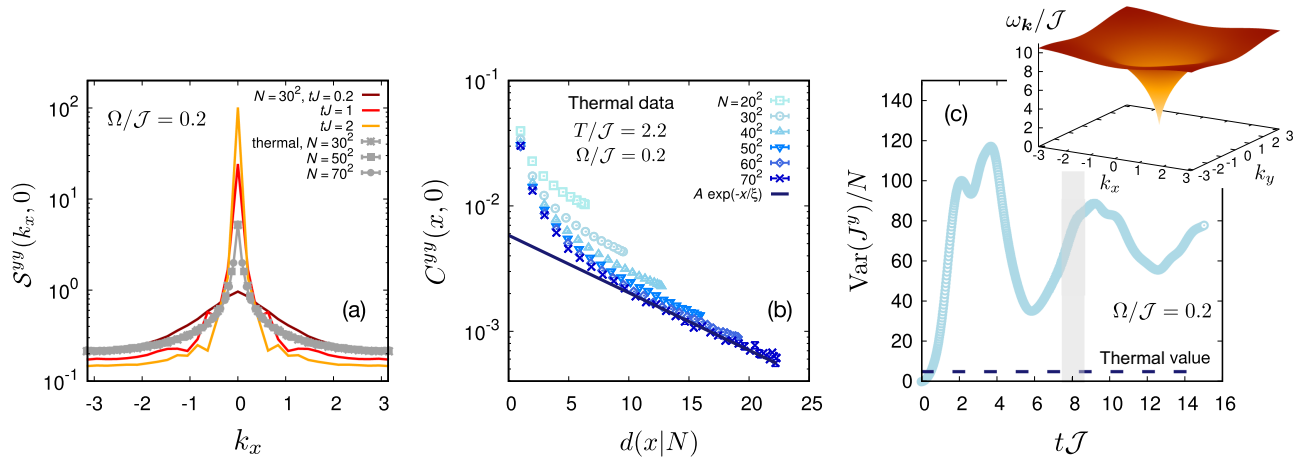


FIG. 8. TaT dynamics vs thermalization. (a) Evolution of the structure factor $\mathcal{S}^{yy}(\boldsymbol{k})$ at three different times for $\Omega/\mathcal{J} = 0.2$ and $N = 30^2$ obtained via dTWA. The time-dependent results are compared to thermal data (at $T/\mathcal{J} = 2.2$) for three different sizes (including the one of the dynamical calculation): Lack of scaling of the thermal structure factor indicates that the system at equilibrium is in a paramagnetic phase. (b) Correlations at thermal equilibrium (from QMC) for various system sizes, plotted as a function of the chord length $d(x|N) = (\sqrt{N}/\pi)\sin(\pi x/\sqrt{N})$. The solid line is an exponential fit, providing an estimate for the correlation length $\xi \approx 9.5$. (c) Time evolution of the structure factor peak $\mathcal{S}^{yy}(\boldsymbol{k} = 0) = \mathrm{Var}(J^y)/N$ for $\Omega/\mathcal{J} = 0.2$ and $N = 30^2$, obtained via dTWA, and compared with the thermal value $\mathcal{S}^{yy}(\boldsymbol{k} = 0) \approx 5.2$. The gray shaded area corresponds to the time at which correlations spreading at the average group velocity of spin waves (whose dispersion relation is represented in the inset) should have reached the distance 2ξ.

Standard thermalization of two-point correlation properties in a nonintegrable system would be expected when correlations spreading through the system reach a length comparable to the equilibrium correlation length ξ. Our model admits well-defined spin-wave excitations above its ground state, with a dispersion relation $\omega_{\boldsymbol{k}}$ shown in the inset of Fig. 8(c)—corresponding to Eq. (B5) with $\Omega \to -\Omega$, when building spin-wave theory on top of the coherent spin state aligned with the field. If the spreading of correlations in our system were caused by the propagation of spin-wave quasiparticles, correlations would develop around each point within a light cone with a linear size $d(t) \approx 2v_g t$ [8], where v_g is a characteristic group velocity of the excitations. Here we estimate v_g as the average group velocity over the Brillouin zone (BZ), $\bar{v}_g = N^{-1}\sum_{\boldsymbol{k}\in \mathrm{BZ}} |\nabla_{\boldsymbol{k}}\omega_{\boldsymbol{k}}|$, giving $\bar{v}_g \approx 1.19\mathcal{J}$ for the above cited parameters. With this information at hand, one could naively estimate the equilibration time for the correlations in the system as that at which, e.g., $d(t^*) \approx 2\xi$; namely, $t^* \approx \xi/v_g$. On the other hand, as shown in Fig. 8(c), at the time in question, as well as for significantly later times, correlations remain long-ranged—namely, the peak in the structure factor $\mathcal{S}^{yy}(0)$ remains of order $O(N)$ [corresponding to $\mathrm{Var}(J^y) \sim O(N^2)$] instead of decreasing to a value $O(1)$.

It is clear that, for a model whose equilibrium behavior exhibits long-range order at low energy or temperature, pure-state dynamics thermalizing to a long-range ordered behavior is accompanied by the onset of long-range multipartite entanglement. Moreover, recent works [42,43] have shown that scalable entanglement in the form of spin squeezing can also appear as a transient effect in this dynamics, before the onset of long-range or quasi-long-range order. These results might erroneously suggest that the existence of long-range order in the equilibrium phase diagram of a model is a necessary condition for it to produce scalable multipartite entanglement in its dynamics. Here we clearly show that this is not the case. Even Hamiltonians with short-range correlations for any temperature or energy at equilibrium, such as the one considered here, can induce long-range entanglement in the dynamics—provided of course that the dynamics avoid thermalization over sizable timescales. TaT dynamics in XY models offers a relevant example in this direction.

3. *Crossover in the scaling and spin-wave instabilities*

When comparing the scaling of the maximum of $\mathrm{Var}(J^y)$ between the all-to-all case [Fig. 5(c)] and the 2D dipolar case (Fig. 9) a clear difference emerges. In the dipolar case, Heisenberg scaling of the peak of $\mathrm{Var}(J^y)$ (as well as of the other collective-spin components) fails to persist after reaching a given system size—the smaller the larger the field. As seen in Fig. 9, dTWA predicts a well-defined crossover from Heisenberg scaling of the $\mathrm{Var}(J^y)$ peak to sub-Heisenberg scaling. This is a rather unconventional effect, which further underscores the nonequilibrium nature of the correlations associated with $\mathrm{Var}(J^y)$ dynamics. To quantitatively understand this crossover, we report its onset on the (Ω, L) plane in Fig. 4: There we observe that the crossover line follows the same behavior as the line separating the regime of stable TaT dipolar dynamics from that of unstable dynamics due to the emergence of

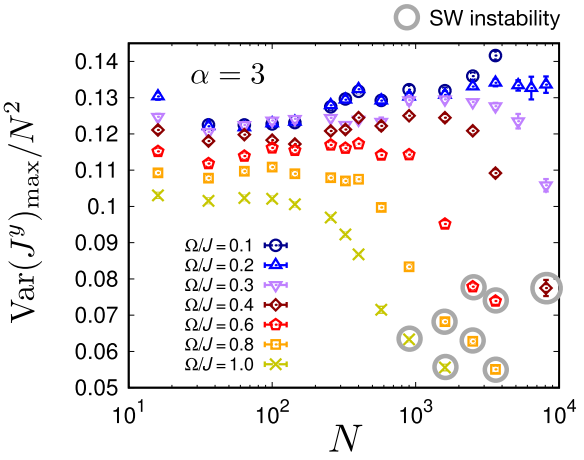


FIG. 9. Heisenberg scaling of entanglement and its breakdown. Scaling of the peak of $\mathrm{Var}(J^y)$ for $\alpha = 3$. As in Fig. 3, the gray circles highlight field and size values at which imaginary spin-wave frequencies appear.

imaginary spin-wave frequencies. Therefore we conclude that the crossover in the scaling of the correlation peak relates to the onset of spin-wave instabilities, which appear to induce a strong deviation of the TaT dynamics in systems with power-law interactions compared to the case of all-to-all interactions. Spin-wave instabilities for large system sizes may also provide the mechanism by which TaT dynamics with power-law interactions eventually relaxes to a behavior aligning with its equilibrium thermodynamics for local observables [1].

VI. CONCLUSIONS

In this work we have shown how twist-and-turn dynamics in quantum spin Hamiltonians can lead to an exponential onset of entanglement in the form of squeezing at early times, and in the form of long-range correlations, transverse to the axis of initial polarization of the collective spin, at later times. Both observations are associated with scalable multipartite entanglement, which can be certified, as well as potentially exploited, using metrological criteria. Indeed squeezing is of immediate relevance to Ramsey interferometry [29]. Moreover, TaT dynamics has the special property of being constrained to a well-defined parity sector of the J^x collective-spin component. Under this condition, the emergence of long-range correlations transverse to J^x (e.g., for the S^y spin components) translates into an enhanced sensitivity of the above parity to rotations around the transverse axis (e.g., the J^y one), saturating the bound offered by the quantum Fisher information, and therefore reaching Heisenberg scaling in the TaT dynamics [26]. The exponentially fast entanglement dynamics described above is observed for the quantum XY model both with all-to-all interactions as well as for dipolar interactions in 2D. In the latter case, in spite of the model not being integrable, the observed entangling dynamics is at odds with thermalization, which would instead lead to an inversion of the collective spin without the development of long-range correlations.

When compared with the paradigmatic one-axis-twisting dynamics, TaT dynamics offers an exponential acceleration of the onset of quantum correlations. The latter can be an asset for several experimental platforms with power-law interactions (neutral atoms and molecules, trapped ions, nitrogen vacancies, etc.). It can potentially lead to generating entanglement at a faster rate than that related to the coupling of the system to its environment, therefore increasing drastically the number of degrees of freedom that can be entangled within the coherence time of the experiment. For weakly long-ranged interactions ($\alpha \geq D$, as, e.g., in the case of dipolar systems) TaT dynamics is subject to instabilities for system sizes exceeding a threshold which is field dependent, and which diverges when the field vanishes. On the other hand, for strongly long-ranged interactions ($\alpha < D$, as realized, e.g., using trapped ions and atoms in cavities) we predict that TaT dynamics is not affected by instabilities up to the largest possible sizes. Porting TaT dynamics to platforms which offer single-site addressing is very appealing, since it would directly enable the optimal certification of multipartite entanglement with Heisenberg scaling by using the spin parity. The latter is instead inaccessible in setups using, e.g., atomic clouds in cavities [5].

All numerical simulations have been performed on the CBPsmn cluster at the ENS of Lyon.

Note added. Recently, we became aware of two works [44,45] which exhibit time-independent Hamiltonians saturating algebraic (not exponential) Lieb-Robinson bounds for quantum-state transfer in systems of free particles with power-law hopping, and time-independent protocols saturating exponential Lieb-Robinson bounds at the cost of introducing ancilla qubits whose number (per system's qubit) grows logarithmically with system size. These works highlight the importance of devising time-independent protocols which achieve time optimality for the flow of quantum information in the case of power-law interactions.

ACKNOWLEDGMENTS

T. R. and F. M. acknowledge the support of ANR (ANR-22-PETQ-0004 France 2030, project QuBitAF). M. K. acknowledges the support from the Applied Quantum Computing Challenge Program at the National Research Council of Canada. A. C. acknowledges support from the Canada First Research Excellence Fund and the Natural Sciences and Engineering Research Council of Canada. We thank Ana Maria Rey for pointing out Ref. [30] to us. M. K. acknowledges useful discussions with Christopher Wyenberg, Kent Ueno, and Manuel Muñoz-Arias.

DATA AVAILABILITY

There are no publicly available research data or software supporting this article. Requests for further information or data should be sent to the authors.

APPENDIX A: FROM THE TWIST-AND-TURN HAMILTONIAN TO THE SQUEEZING HAMILTONIAN

In this appendix, we focus on the case of the all-to-all interactions ($\alpha = 0$), and we connect the TaT Hamiltonian with the squeezing Hamiltonian of quantum optics via a linearized spin-boson transformation. The twist-and-turn Hamiltonian with $\alpha = 0$ for N spins with $S = 1/2$ can be written in terms of the collective spin components as

$$H(\Omega) = \frac{(J^z)^2}{2I} + \Omega J^x + \text{const}, \tag{A1}$$

where we have assumed that the collective spin length is maximal, $\boldsymbol{J}^2 = N/2(N/2+1)$, and therefore treated it as constant. Here the coupling constant reads $[1/(2I)] = (\mathcal{J}/N)$, to connect it with the notation of Eq. (1).

In the following, we outline the spin-to-boson mapping, recall the general properties of the squeezing Hamiltonian in quantum optics, and show how the bosonic Hamiltonian—onto which the TaT Hamiltonian can be transformed—can, in general, be cast into the form of a squeezing Hamiltonian. This will allow us to deduce analytically the squeezing dynamics at short times, and to prove that the squeezed and antisqueezed collective-spin components evolve exponentially at a rate $\lambda = \sqrt{\Omega(\mathcal{J}-\Omega)}$.

1. Spin-to-boson mapping

The above Hamiltonian can be mapped onto a quadratic single-mode bosonic Hamiltonian, with operators $a, a^\dagger$, via the (linearized) Holstein-Primakoff transformation,

$$\begin{aligned} J^x &= \frac{N}{2} - a^\dagger a, \\ J^y &\approx \frac{\sqrt{N}}{2}(a + a^\dagger), \\ J^z &\approx \frac{\sqrt{N}}{2i}(a - a^\dagger), \end{aligned} \tag{A2}$$

to give

$$\begin{aligned} H(\Omega) &\approx H_b(\Omega, a, a^\dagger) \\ &= \frac{\Omega N}{2} + \frac{N}{8I} - \frac{N}{8I}[a^2 + (a^\dagger)^2] \\ &\quad + \left(\frac{N}{4I} - \Omega\right) a^\dagger a + \text{const}. \end{aligned} \tag{A3}$$

This mapping is valid as long as the dynamics does not lead to a large deviation in the evolved state from the initial coherent spin state, such that $\langle J^x \rangle \lesssim N/2$, or $\langle a^\dagger a \rangle \ll N$.

The above Hamiltonian reduces to the well-known *squeezing Hamiltonian* in quantum optics, $H = -[N/(8I)][a^2 + (a^\dagger)^2]$, at the optimal field,

$$\Omega_0 = \frac{N}{4I} = \frac{\mathcal{J}}{2}. \tag{A4}$$

The bosonic Hamiltonian (*not* the spin Hamiltonian) has a fundamental *symmetry*. If one reflects the field around the optimal value,

$$\Omega \to 2\Omega_0 - \Omega, \tag{A5}$$

and rotates the phase of the bosonic operators by $\pi/2$, namely, $\tilde{a} = e^{i\pi/2}a$, then

$$H_b(2\Omega_0 - \Omega, \tilde{a}, \tilde{a}^\dagger) = -H_b(\Omega, a, a^\dagger) + \text{const}, \tag{A6}$$

up to an irrelevant constant. The Hamiltonian is real valued in the Fock basis $|n\rangle$. When starting the evolution from a real-valued state in this basis—such as the vacuum, which corresponds to the coherent spin state $\otimes_i |\rightarrow_i\rangle$—the subsequent evolution is time-reversal invariant, meaning that quantities that are also real-valued operators on the Fock basis have the same evolution under H as under $-H$ [10]. Hence the transformation $\Omega \to 2\Omega_0 - \Omega$ and $\tilde{a} = e^{i\pi/2}a$ leaves the evolution unchanged, provided that one is comparing bosonic observables which are appropriately transformed (or are time-reversal symmetric).

2. Optimal field and bosonic squeezing

At $\Omega = \Omega_0$ the bosonic Hamiltonian takes the squeezing form,

$$H_b(\Omega_0, a, a^\dagger) = -\frac{N}{8I}[a^2 + (a^\dagger)^2] + \text{const}, \tag{A7}$$

and the evolution operator is the squeezing operator,

$$\begin{aligned} U(t) &= \exp[-iH_b(\Omega_0, a, a^\dagger)t] \\ &= \exp\left(\frac{q}{2}(a^\dagger)^2 - \frac{q^*}{2}a^2\right) = S(q), \end{aligned} \tag{A8}$$

with squeezing parameter $q = i[(Nt)/(4I)] = \eta e^{i\phi}$, where $\eta = Nt/(4I) = \mathcal{J}t/2$ and $\phi = \pi/2$.

As customarily done in quantum optics [46], we introduce the generalized mode quadrature,

$$X_\theta = \frac{e^{-i\theta}a + e^{i\theta}a^\dagger}{\sqrt{2}} = \cos\theta\, X + \sin\theta\, P, \tag{A9}$$

where $X = X_0 = (a + a^\dagger)/\sqrt{2}$ and $P = X_{\pi/2} = (a - a^\dagger)/(i\sqrt{2})$. The application of the squeezing operator with $q = i\eta$ on the vacuum gives rise to a squeezed vacuum state, with a squeezed and antisqueezed quadrature:

$$\mathrm{Var}(X_{\pi/4}) = \frac{e^{2\eta}}{2}, \qquad \mathrm{Var}(X_{3\pi/4}) = \frac{e^{-2\eta}}{2}. \tag{A10}$$

Moving back to spins, we obtain

$$J^y \approx \sqrt{\frac{N}{2}}X, \qquad J^z \approx \sqrt{\frac{N}{2}}P, \tag{A11}$$

so that

$$\mathrm{Var}\left(\frac{J^y + J^z}{\sqrt{2}}\right) \approx \frac{N}{4}e^{2\lambda t}, \qquad \mathrm{Var}\left(\frac{J^y - J^z}{\sqrt{2}}\right) \approx \frac{N}{4}e^{-2\lambda t}, \tag{A12}$$

where we have used the property $\eta = \lambda t = \mathcal{J}t/2$ at the optimal field Ω_0.

On the other hand, the boson population evolves as

$$\langle a^\dagger a\rangle = \sinh(\eta), \tag{A13}$$

yielding the spin squeezing parameter

$$\xi_R^2 = \frac{N\mathrm{Var}(\frac{J^y - J^z}{\sqrt{2}})}{\langle J^x\rangle^2} \approx \frac{e^{-2\eta}}{[1 - \frac{2}{N}\sinh(\eta)]^2}. \tag{A14}$$

This result shows the *exponential* onset of spin squeezing, and of exponential growth of the quantum Fisher information for the antisqueezed component, within the time frame of validity of the linearized spin-boson transformation—i.e., as long as $\langle a^\dagger a\rangle = \sinh(\eta) \ll N$.

3. Squeezing away from the optimal field

Away from the optimal field, the bosonic Hamiltonian has the form

$$H_b = -\frac{\chi}{2}[(a^\dagger)^2 + a^2] - \frac{\delta}{2}(a^\dagger a + aa^\dagger), \tag{A15}$$

where $\chi = [N/(4I)] = \mathcal{J}/2$ and $\delta = \Omega - \Omega_0$. We now want to transform it into the squeezing Hamiltonian,

$$H_b = -\frac{\zeta}{2}[(b^\dagger)^2 + b^2] + \mathrm{const}, \tag{A16}$$

via a *squeezing* Bogolyubov transformation:

$$a = ub - vb^\dagger, \qquad b = ua + va^\dagger. \tag{A17}$$

The transformation (with $|u|^2 - |v|^2 = 1$ to conserve the commutation relations) reads

$$u = \sqrt{\frac{1}{2}\left(\frac{\chi}{\zeta} + 1\right)}, \qquad v = \mathrm{sgn}(\delta)\sqrt{\frac{1}{2}\left(\frac{\chi}{\zeta} - 1\right)}, \tag{A18}$$

where

$$\zeta = \sqrt{\chi^2 - \delta^2} = \sqrt{\Omega(\mathcal{J} - \Omega)} = \lambda. \tag{A19}$$

This transformation leads to *real* coefficients u and v under the condition

$$|\delta| \le \chi \to |\Omega - \Omega_0| \le \Omega_0 \quad \text{or} \quad \Omega \in [0, 2\Omega_0]. \tag{A20}$$

We shall restrict our attention to this interval, although the calculation can be generalized to values outside of it.

The bosonic operators $b, b^\dagger$ are squeezed by $S(i\lambda t) = e^{-iH_b t}$ as [46]

$$b(\lambda t) = S^\dagger b S = b\cosh(\lambda t) + i\sinh(\lambda t)b^\dagger, \tag{A21}$$

hence the transformation of the a operator reads:

$$\begin{aligned} a(\lambda) &= ub(\lambda t) - vb^\dagger(\lambda t) \\ &= \left[\cosh(\lambda t) + i\frac{\delta}{\lambda}\sinh(\lambda t)\right]a + i\frac{\chi}{\lambda}\sinh(\lambda t)a^\dagger. \end{aligned} \tag{A22}$$

After a lengthy but straightforward calculation, we obtain that the fluctuations of the generalized quadrature X_θ take the form

$$\begin{aligned} \langle X_\theta^2\rangle = {} & \frac{1}{2}\frac{\delta}{\lambda^2}[-\delta + \chi\cos(2\theta)] \\ & + \frac{1}{4}\frac{\chi}{\lambda}\left[\frac{\chi}{\lambda} + \sin(2\theta) - \frac{\delta}{\lambda}\cos(2\theta)\right]e^{2\lambda t} \\ & + \frac{1}{4}\frac{\chi}{\lambda}\left[\frac{\chi}{\lambda} - \sin(2\theta) - \frac{\delta}{\lambda}\cos(2\theta)\right]e^{-2\lambda t}, \end{aligned} \tag{A23}$$

which reproduces Eq. (A10) when taking $\delta = 0$ and $\theta = \{\pi/4, 3\pi/4\}$.

We observe the fundamental symmetry, highlighted in Sec. A 1:

$$\begin{aligned} &\delta \to -\delta, \\ &\theta \to \theta + \pi/2, \\ &t \to -t. \end{aligned} \tag{A24}$$

The boson number takes the form

$$\langle a^\dagger a\rangle = \left(\frac{\chi}{\lambda}\right)^2 \sinh^2(\lambda t), \tag{A25}$$

so that the spin squeezing parameter is

$$\xi_R^2 \approx \frac{2\min_\theta \langle X_\theta^2 \rangle}{\left[1 - \frac{2}{N}\left(\frac{\chi}{\lambda}\right)^2 \sinh^2(\lambda t)\right]^2}. \tag{A26}$$

The above result [Eq. (A23)] shows that the antisqueezed component of the collective spin grows exponentially as $e^{2\lambda t}$. At short time the state is of minimal uncertainty, so that the corresponding squeezed component decreases exponentially as $e^{-2\lambda t}$.

4. Short-time behavior

The short-time expansion of $\langle X_\theta^2 \rangle$ reads

$$\langle X_\theta^2 \rangle \approx \frac{1}{2}[1 + 2\chi t \sin(2\theta) + 2(\chi t)^2 - 2\delta\chi t^2 \cos(2\theta) + O(t^3)], \tag{A27}$$

and that of the spin squeezing parameter reads

$$\xi_R^2 \approx \frac{1 - 2\chi t + O(t^2)}{\left(1 - \frac{2\chi^2 t^2}{N} + O(t^4)\right)^2}; \tag{A28}$$

namely, the dependence on δ (i.e., on the field) of the quadrature fluctuations and of the squeezing parameter appears only in *quadratic terms* in time, $O(t^2)$. This implies that the time dependence of the squeezing parameter at short time is the same regardless of δ—as long as it satisfies the condition of Eq. (A20). This result encompasses also the case $\delta = -\chi$ (i.e., $\Omega = 0$) corresponding to the one-axis-twisting dynamics.

5. Comparison between bosonic squeezing and spin squeezing

Figure 10 presents an extended comparison between the predictions for squeezing from the bosonic model, Eq. (A26), and the full TaT dynamics for $\alpha = 0$.

We observe that the bosonic model predicts the correct squeezing dynamics down to the optimal squeezing, and in particular the Ω-dependent exponential behavior which emerges after the Ω-independent transient at short times (see previous subsection). Related to this crossover between short- and intermediate-time squeezing dynamics, there is an apparent change in the exponential decay dynamics of squeezing from a faster to a slower decay, observed at sufficiently small fields. This property, captured by the bosonic model for the case $\alpha = 0$, is also seen in the case of the dipolar dynamics in 2D, as shown in Fig. 3(b).

In spite of its predictive power, the linearized bosonic model completely misses the value of the optimal squeezing observed for the spin model. We can therefore conclude that the observed optimal squeezing value stems fundamentally from the nonlinear nature of the spin dynamics on the Bloch sphere.

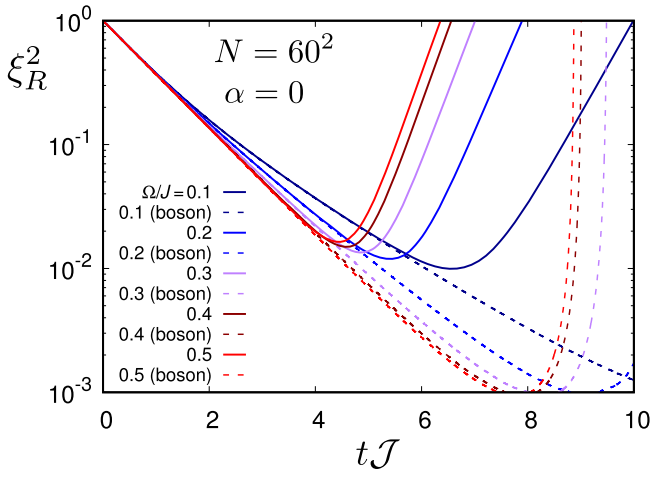


FIG. 10. Squeezing dynamics of the all-to-all TaT model for various fields (solid lines) compared with the predictions from the linearized bosonic approximation, Eq. (A26) (dashed lines).

APPENDIX B: ROTOR-SPIN-WAVE THEORY FOR THE TaT HAMILTONIAN

Rotor-spin-wave theory [38,40] describes the dynamics of a quantum spin model in terms of two sets of variables: a rotor variable, which describes the dynamics projected onto the sector of Dicke states with maximal spin length $\boldsymbol{J}^2 = N/2(N/2+1)$, and spin-wave variables, which describe in a linearized fashion the dynamics leaking out of the Dicke sector. The theory relies on the fundamental (approximate) assumption that the two dynamics can be considered as decoupled, and it is valid under the condition that the population of the spin-wave modes remains small, allowing one to justifiably neglect the coupling between the spin waves and the rotor variable.

Following the prescription of Refs. [38,40], we rewrite the TaT Hamiltonian, Eq. (1), as $H \approx H_{\mathrm{R}} + H_{\mathrm{SW}}$. Here,

$$\begin{aligned} H_{\mathrm{R}} &= -\frac{1}{2I}[(K^x)^2 + (K^y)^2] + \Omega K^x \\ &= \frac{(K^z)^2}{2I} + \Omega K^x + \mathrm{const} \end{aligned} \tag{B1}$$

is the rotor Hamiltonian, where $\boldsymbol{K}$ is an angular momentum variable with $\boldsymbol{K}^2 = N/2(N/2+1)$ and

$$\frac{1}{2I} = \frac{\mathcal{J}\gamma_0}{N-1} \tag{B2}$$

is the effective inverse moment of inertia, with

$$\gamma_{\boldsymbol{k}} = \sum_{\boldsymbol{r}\neq 0} \frac{e^{i\boldsymbol{k}\cdot\boldsymbol{r}}}{r^\alpha}. \tag{B3}$$

Moreover,

$$H_{\mathrm{SW}} = \sum_{\boldsymbol{k}\neq 0} \omega_{\boldsymbol{k}} b_{\boldsymbol{k}}^{\dagger} b_{\boldsymbol{k}} + \mathrm{const} \tag{B4}$$

is the spin-wave Hamiltonian, where $b_{\boldsymbol{k}}, b_{\boldsymbol{k}}^{\dagger}$ are Bogolyubov bosons diagonalizing the (linearized) bosonic Hamiltonian onto which the spin Hamiltonian is mapped via the Holstein-Primakoff transformation, and $\omega_{\boldsymbol{k}} = \sqrt{A_{\boldsymbol{k}}^2 - B_{\boldsymbol{k}}^2}$ is the dispersion relation of the spin waves built around the initial coherent spin state, where [38]

$$A_{\boldsymbol{k}} = \mathcal{J}(\gamma_0 - \gamma_{\boldsymbol{k}}/2) - \Omega, \qquad B_{\boldsymbol{k}} = -\mathcal{J}\gamma_{\boldsymbol{k}}/2. \tag{B5}$$

The rotor Hamiltonian has the structure of a TaT Hamiltonian with $\alpha = 0$, and therefore it drives squeezing dynamics with an exponential rate $\lambda_{\mathrm{eff}} = \sqrt{\Omega(\mathcal{J}_{\mathrm{eff}} - \Omega)}$, where

$$\mathcal{J}_{\mathrm{eff}} = \frac{N}{2I} = \frac{N\mathcal{J}\gamma_0}{N-1}. \tag{B6}$$

When $\Omega = 0$, the spin-wave dispersion relation $\omega_{\boldsymbol{k}}$ has the characteristic structure of a gapless Goldstone mode, associated with the U(1) symmetry of the Hamiltonian. Upon application of the field, the frequency at zero wave vector becomes imaginary, namely, $\omega_0 = \sqrt{-\Omega(\mathcal{J}\gamma_0 - \Omega)} \approx i\lambda_{\mathrm{eff}}$ (for $N \gg 1$), reflecting the fact that the coherent spin state becomes an unstable fixed point of the dynamics. Yet, for sufficiently big sizes, also finite-wave-vector spin-wave modes—which are the ones properly appearing in RSW theory—can acquire imaginary frequencies. On a $L \times L$ square lattice, this occurs first for the smallest wave vector $\boldsymbol{k} = (2\pi/L, 0)$ when $A_{(2\pi/L,0)}^2 < B_{(2\pi/L,0)}^2$, namely,

$$\frac{\Omega}{\mathcal{J}} > \gamma_0 - \gamma_{2\pi/L,0} \sim L^{-2z} \quad (L \gg 1), \tag{B7}$$

where $z = 1$ for $\alpha \geq D+2$, $z = (\alpha - D)/2$ for $D < \alpha < D+2$, and $z = 0$ for $\alpha \leq D$ [39]. For the dipolar interactions ($\alpha = 3$) in $D = 2$, which we have treated in this work, $z = 1/2$, so that the critical value of the field generating imaginary frequencies for finite-$\boldsymbol{k}$ spin waves goes as L^{-1}—precisely the behavior shown in Fig. 4. Interestingly, for $\alpha < D$, the critical field for the onset of spin-wave instabilities does not scale with system size, meaning that there is an entire range of field values for which TaT dynamics is stable up to the thermodynamic limit, even though the system is not integrable, and even though the TaT dynamics producing squeezing and Heisenberg scaling of collective-spin fluctuations is incompatible with thermalization.

On the other hand, the emergence of imaginary spin-wave frequencies leads to an exponential divergence of the populations of Holstein-Primakoff bosons, and to the breakdown of the RSW approach. Yet this breakdown occurs over timescales which are comparable with the inverse exponential divergence rate:

$$\begin{aligned}\lambda_{\boldsymbol{k}} &= \sqrt{|A_{\boldsymbol{k}}^2 - B_{\boldsymbol{k}}^2|} \\ &= \sqrt{|\omega_{\boldsymbol{k}}^2(\Omega = 0) - \Omega[\mathcal{J}(2\gamma_0 - \gamma_{\boldsymbol{k}}) - \Omega]|}.\end{aligned} \tag{B8}$$

It is easy to observe that $\lambda_{\boldsymbol{k}} < \lambda_{\mathrm{eff}} = \lambda_{\boldsymbol{k}=0}$ for any finite $\boldsymbol{k}$, namely, the rotor dynamics is systematically faster than the spin-wave dynamics, even in the presence of spin-wave instabilities. This mechanism may be responsible for the persistent scalability of squeezing observed in our simulations, even for system sizes and fields for which spin-wave instabilities (in the form of imaginary frequencies) are present.

APPENDIX C: MAGNETIZATION DYNAMICS FOR LARGE SYSTEM SIZES AND FIELDS

As seen in Sec. III, the dipolar system in 2D appears to exhibit a field-dependent scaling of optimal squeezing, at variance with the universal scaling $(\xi_R^2)_{\mathrm{min}} \sim N^{-1/2}$ seen in the $\alpha = 0$ case. This could be interpreted as a consequence of the presence of spin-wave instabilities in the dipolar system, which are instead nonexistent for $\alpha = 0$ (in fact for any $\alpha < D$, as we argued in Sec. IV and in the previous section). Nonetheless, this interpretation is incorrect. In the case of the dipolar interactions in 2D, and for all the system sizes studied in this work, the magnetization of the squeezed collective-spin component does not show any sign of instability over the timescale of squeezing dynamics. We illustrate this point by choosing the cases $\Omega/\mathcal{J} = 0.6$ and $\Omega/\mathcal{J} = 0.8$, which clearly possess spin-wave instabilities for the larger system size we investigated (see Sec. IV).

Within RSW theory, the magnetization should behave as $\langle J^x \rangle = \langle K^x \rangle - \sum_{\boldsymbol{k}\neq 0} \langle a_{\boldsymbol{k}}^{\dagger} a_{\boldsymbol{k}} \rangle$, where K^x is the x component of the rotor variable introduced in Appendix B, following the all-to-all TaT dynamics, and $a_{\boldsymbol{k}}, a_{\boldsymbol{k}}^{\dagger}$ are Holstein-Primakoff bosons, related to the previously cited $b_{\boldsymbol{k}}, b_{\boldsymbol{k}}^{\dagger}$ bosons via a Bogolyubov transformation. A spin-wave instability would correspond to an exponential increase of the bosonic populations $\langle a_{\boldsymbol{k}}^{\dagger} a_{\boldsymbol{k}} \rangle$, corresponding to the wave vectors developing an imaginary frequency, and hence, to an exponential decrease of the magnetization. On the other hand, this behavior is not observed over the timescales of squeezing dynamics, as shown in Fig. 11. There we see that the magnetization remains macroscopic over timescales growing as $\log N$, i.e., the same behavior as in the case of smaller fields. This means that the change in the scaling of squeezing compared to the all-to-all TaT dynamics is fundamentally driven by the dynamics of the squeezed

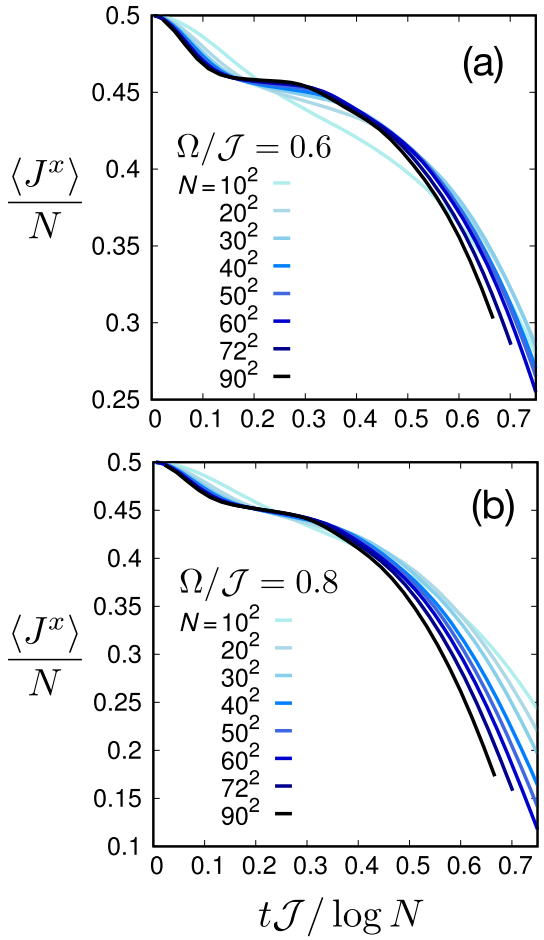


FIG. 11. Magnetization dynamics in the dipolar 2D system at large fields: (a) $\Omega = 0.6\mathcal{J}$ and (b) $\Omega = 0.8\mathcal{J}$. All data are from dTWA calculations.

component of the collective spin transverse to the magnetization, which becomes field dependent.

At the same time, it is interesting to observe that, after a size-independent plateau over times $\sim \log N$, the dynamics of the magnetization of the collective spin at larger fields starts showing significant differences with that observed at low fields [comparing Fig. 11 with Fig. 3(a)]. Indeed the depolarization dynamics becomes faster (in time units $\sim \log N$) the larger the system size, likely a manifestation of the spin-wave instability. Investigating the nature of this dynamics at longer times, and the conditions under which it can lead to thermalization, will be the subject of future work.

[1] L. D'Alessio, Y. Kafri, A. Polkovnikov, and M. Rigol, *From quantum chaos and eigenstate thermalization to statistical mechanics and thermodynamics*, Adv. Phys. **65**, 239 (2016).

[2] A. M. Kaufman, M. E. Tai, A. Lukin, M. Rispoli, R. Schittko, P. M. Preiss, and M. Greiner, *Quantum thermalization through entanglement in an isolated many-body system*, Science **353**, 794 (2016).

[3] D. A. Abanin, E. Altman, I. Bloch, and M. Serbyn, *Colloquium: Many-body localization, thermalization, and entanglement*, Rev. Mod. Phys. **91**, 021001 (2019).

[4] M. Gärttner, J. G. Bohnet, A. Safavi-Naini, M. L. Wall, J. J. Bollinger, and A. M. Rey, *Measuring out-of-time-order correlations and multiple quantum spectra in a trapped-ion quantum magnet*, Nat. Phys. **13**, 781 (2017).

[5] Z. Li, S. Colombo, C. Shu, G. Velez, S. Pilatowsky-Cameo, R. Schmied, S. Choi, M. Lukin, E. Pedrozo-Peñafiel, and V. Vuletić, *Improving metrology with quantum scrambling*, Science **380**, 1381 (2023).

[6] S. Xu and B. Swingle, *Scrambling dynamics and out-of-time-ordered correlators in quantum many-body systems*, PRX Quantum **5**, 010201 (2024).

[7] C.-F. A. Chen, A. Lucas, and C. Yin, *Speed limits and locality in many-body quantum dynamics*, Rep. Prog. Phys. **86**, 116001 (2023).

[8] M. Cheneau, P. Barmettler, D. Poletti, M. Endres, P. Schauß, T. Fukuhara, C. Gross, I. Bloch, C. Kollath, and S. Kuhr, *Light-cone-like spreading of correlations in a quantum many-body system*, Nature (London) **481**, 484 (2012).

[9] G. Carleo, F. Becca, L. Sanchez-Palencia, S. Sorella, and M. Fabrizio, *Light-cone effect and supersonic correlations in one- and two-dimensional bosonic superfluids*, Phys. Rev. A **89**, 031602(R) (2014).

[10] I. Frérot, P. Naldesi, and T. Roscilde, *Multispeed prethermalization in quantum spin models with power-law decaying interactions*, Phys. Rev. Lett. **120**, 050401 (2018).

[11] L. Cevolani, J. Despres, G. Carleo, L. Tagliacozzo, and L. Sanchez-Palencia, *Universal scaling laws for correlation spreading in quantum systems with short- and long-range interactions*, Phys. Rev. B **98**, 024302 (2018).

[12] M. B. Hastings and T. Koma, *Spectral gap and exponential decay of correlations*, Commun. Math. Phys. **265**, 781 (2006).

[13] M. C. Tran, A. Y. Guo, C. L. Baldwin, A. Ehrenberg, A. V. Gorshkov, and A. Lucas, *Lieb-Robinson light cone for power-law interactions*, Phys. Rev. Lett. **127**, 160401 (2021).

[14] M. C. Tran, A. Y. Guo, A. Deshpande, A. Lucas, and A. V. Gorshkov, *Optimal state transfer and entanglement generation in power-law interacting systems*, Phys. Rev. X **11**, 031016 (2021).

[15] A. Polkovnikov, K. Sengupta, A. Silva, and M. Vengalattore, *Colloquium: Nonequilibrium dynamics of closed interacting quantum systems*, Rev. Mod. Phys. **83**, 863 (2011).

[16] A. Micheli, D. Jaksch, J. I. Cirac, and P. Zoller, *Many-particle entanglement in two-component Bose-Einstein condensates*, Phys. Rev. A **67**, 013607 (2003).

[17] W. Muessel, H. Strobel, D. Linnemann, T. Zibold, B. Juliá-Díaz, and M. K. Oberthaler, *Twist-and-turn spin squeezing in Bose-Einstein condensates*, Phys. Rev. A **92**, 023603 (2015).

[18] G. Sorelli, M. Gessner, A. Smerzi, and L. Pezzè, *Fast and optimal generation of entanglement in bosonic Josephson junctions*, Phys. Rev. A **99**, 022329 (2019).

[19] M. H. Muñoz-Arias, I. H. Deutsch, and P. M. Poggi, *Phase-space geometry and optimal state preparation in quantum metrology with collective spins*, PRX Quantum **4**, 020314 (2023).

[20] Y. Chu, X. Li, and J. Cai, *Quantum delocalization on correlation landscape: The key to exponentially fast multipartite entanglement generation*, Phys. Rev. Lett. **133**, 110201 (2024).
[21] H. Strobel, W. Muessel, D. Linnemann, T. Zibold, D. B. Hume, L. Pezzè, A. Smerzi, and M. K. Oberthaler, *Fisher information and entanglement of non-Gaussian spin states*, Science **345**, 424 (2014).
[22] A. Browaeys and T. Lahaye, *Many-body physics with individually controlled Rydberg atoms*, Nat. Phys. **16**, 132 (2020).
[23] L. Chomaz, I. Ferrier-Barbut, F. Ferlaino, B. Laburthe-Tolra, B. L. Lev, and T. Pfau, *Dipolar physics: A review of experiments with magnetic quantum gases*, Rep. Prog. Phys. **86**, 026401 (2022).
[24] S. L. Cornish, M. R. Tarbutt, and K. R. A. Hazzard, *Quantum computation and quantum simulation with ultracold molecules*, Nat. Phys. **20**, 730 (2024).
[25] C. Monroe, W. C. Campbell, L.-M. Duan, Z.-X. Gong, A. V. Gorshkov, P. W. Hess, R. Islam, K. Kim, N. M. Linke, G. Pagano, P. Richerme, C. Senko, and N. Y. Yao, *Programmable quantum simulations of spin systems with trapped ions*, Rev. Mod. Phys. **93**, 025001 (2021).
[26] I. Frérot and T. Roscilde, *Symmetry: A fundamental resource for quantum coherence and metrology*, Phys. Rev. Lett. **133**, 260402 (2024).
[27] S.-A. Guo, Y.-K. Wu, J. Ye, L. Zhang, W.-Q. Lian, R. Yao, Y. Wang, R.-Y. Yan, Y.-J. Yi, Y.-L. Xu, B.-W. Li, Y.-H. Hou, Y.-Z. Xu, W.-X. Guo, C. Zhang, B.-X. Qi, Z.-C. Zhou, L. He, and L.-M. Duan, *A site-resolved two-dimensional quantum simulator with hundreds of trapped ions*, Nature (London) **630**, 613 (2024).
[28] H. J. Manetsch, G. Nomura, E. Bataille, K. H. Leung, X. Lv, and M. Endres, *A tweezer array with 6100 highly coherent atomic qubits*, Nature (London) **647**, 60 (2025).
[29] L. Pezzè, A. Smerzi, M. K. Oberthaler, R. Schmied, and P. Treutlein, *Quantum metrology with nonclassical states of atomic ensembles*, Rev. Mod. Phys. **90**, 035005 (2018).
[30] B. Juliá-Díaz, T. Zibold, M. K. Oberthaler, M. Melé-Messeguer, J. Martorell, and A. Polls, *Dynamic generation of spin-squeezed states in bosonic Josephson junctions*, Phys. Rev. A **86**, 023615 (2012).
[31] M. Kitagawa and M. Ueda, *Squeezed spin states*, Phys. Rev. A **47**, 5138 (1993).
[32] J. Schachenmayer, A. Pikovski, and A. M. Rey, *Many-body quantum spin dynamics with Monte Carlo trajectories on a discrete phase space*, Phys. Rev. X **5**, 011022 (2015).
[33] J. Thibaut, T. Roscilde, and F. Mezzacapo, *Long-range entangled-plaquette states for critical and frustrated quantum systems on a lattice*, Phys. Rev. B **100**, 155148 (2019).
[34] T. Comparin, F. Mezzacapo, and T. Roscilde, *Robust spin squeezing from the tower of states of U(1)-symmetric spin Hamiltonians*, Phys. Rev. A **105**, 022625 (2022).
[35] F. Caleca, S. Bocini, F. Mezzacapo, and T. Roscilde, *Giant number-parity effect leading to spontaneous symmetry breaking in finite-size quantum spin models*, Phys. Rev. Lett. **135**, 220402 (2025).
[36] T. Comparin, F. Mezzacapo, and T. Roscilde, *Multipartite entangled states in dipolar quantum simulators*, Phys. Rev. Lett. **129**, 150503 (2022).
[37] S. R. Muleady, M. Yang, S. R. White, and A. M. Rey, *Validating phase-space methods with tensor networks in two-dimensional spin models with power-law interactions*, Phys. Rev. Lett. **131**, 150401 (2023).
[38] T. Roscilde, T. Comparin, and F. Mezzacapo, *Entangling dynamics from effective rotor–spin-wave separation in U(1)-symmetric quantum spin models*, Phys. Rev. Lett. **131**, 160403 (2023).
[39] I. Frérot, P. Naldesi, and T. Roscilde, *Entanglement and fluctuations in the XXZ model with power-law interactions*, Phys. Rev. B **95**, 245111 (2017).
[40] T. Roscilde, T. Comparin, and F. Mezzacapo, *Rotor/spin-wave theory for quantum spin models with U(1) symmetry*, Phys. Rev. B **108**, 155130 (2023).
[41] A. W. Sandvik, *Computational studies of quantum spin systems*, AIP Conf. Proc. **1297**, 135 (2010).
[42] M. Block, B. Ye, B. Roberts, S. Chern, W. Wu, Z. Wang, L. Pollet, E. J. Davis, B. I. Halperin, and N. Y. Yao, *Scalable spin squeezing from finite-temperature easy-plane magnetism*, Nat. Phys. **20**, 1575 (2024).
[43] T. Roscilde, F. Caleca, A. Angelone, and F. Mezzacapo, *Scalable spin squeezing from critical slowing down in short-range interacting systems*, Phys. Rev. Lett. **133**, 210401 (2024).
[44] D. Yuan, C. Yin, T. C. Mooney, C. L. Baldwin, A. M. Childs, and A. V. Gorshkov, *Time independence does not limit information flow. I. The free-particle case*, arXiv:2505.18249.
[45] T. C. Mooney, D. Yuan, A. Ehrenberg, C. L. Baldwin, A. V. Gorshkov, and A. M. Childs, *Time independence does not limit information flow. II. The case with ancillas*, arXiv:2505.18254.
[46] G. S. Agarwal, *Quantum Optics* (Cambridge University Press, Cambridge, 2012).